Nuclear Materials and Energy 43 (2025) 101934

Contents lists available at ScienceDirect

Nuclear Materials and Energy

journal homepage: www.elsevier.com/locate/nme

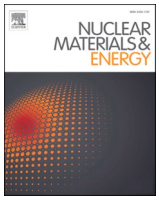

# In-vessel colorimetry of Wendelstein 7-X first wall components after OP2.1☆

G. Motojima [a,b,*], S. Masuzaki [a,b], C.P. Dhard [c], D. Naujoks [c], Mattis Hänel [c], Yu Gao [c], the W7-X Team[1]

[a] National Institute for Fusion Science, National Institutes of Natural Sciences, 322-6 Oroshi-cho, Toki, Gifu 509-5292, Japan
[b] The Graduate University for Advanced Studies, SOKENDAI, 322-6 Oroshi-cho, Toki, Gifu 509-5292, Japan
[c] Max-Planck-Institut für Plasmaphysik, Wendelsteinstrasse 1, 17491 Greifswald, Germany

ARTICLE INFO

*Keywords:*
Colorimetry
W7-X
Deposition layer
Reflection rate

ABSTRACT

Colorimetry has been continuously utilized for the estimation of deposition layer distribution on the first wall panels and divertor target elements in each Operation Phases (OP) of Wendelstein 7-X (W7-X). In OP2.1, significant achievements were made in plasma-wall interaction studies and divertor performance, completed by the installation of actively cooled divertors together with the change of material from fine grain graphite to Carbon Fiber-reinforced Composite. This upgrade enabled the achievement of long-duration plasma discharges, reaching up to 500 s with a total injected energy of 1.3 GJ. Compared to a factor of 2.5 increase in the net average deposition thickness between OP1.2a and 1.2b, no significant change was observed between OP1.2b and OP2.1. The balance of deposition and erosion of deposition layer on the first wall panels is presumably changed in OP2.1. The considerable reasons are discussed qualitatively from the point of possibilities such as lower surface temperature of the divertor target elements, lower impurity level of bulk plasmas, and difference of the location of sputtered carbon source. Moreover, the clear pattern of the colorimetry on the divertor target elements is seen in OP1.2a and OP2.1 not in OP1.2b. However, it is not currently conclusive whether changes in reflectivity and optical properties on the graphite divertor surface are due to erosion or deposition.

## 1. Introduction

Colorimetry is the interdisciplinary scientific technique of quantifying and measuring colors. The colorimetry technique has been also applied to nuclear fusion research [1] mainly for the plasma wall interaction studies by in-situ measurement of deposition layers thickness on the first wall components distributed over a large area. Colorimetry measurements have been conducted in the several fusion devices. In LHD, deposition layer evaluation by colorimetry has revealed the non-uniformity in deposition layer distribution between inside and outside the torus [2]. In QUEST, three types of thickness results, obtained from colorimetry, TEM (Transmission Electron Microscope) and GD-OES (Glow Discharge Optical Emission Spectroscopy), were cross-checked. The results showed that in most positions, colorimetry could derive the minimum possible value of thickness [3]. In W7-X, systematic deposition layer distribution can be evaluated for each Operation Phases (OP) by colorimetry [4]. The thickness of the deposition layer formed in OP1.2b is 2.5 times larger than that formed in OP1.2a, which is comparable to a plasma duration of 2.4 times longer in OP1.2b.

Generally, post-mortem analysis can quantitatively evaluate the deposition layer's thickness by observing the sample's cross-section, e.g. by TEM or GD-OES. Also, the marker layer is a powerful tool for deposition layer evaluation. For example, in TEXTOR, various markers for material transport studies from gaseous high-Z metal carriers such as WF6 and components of sandwich-type marker tiles [5]. In also W7-X, marker layers have been used to evaluate deposition layer [6]. By measuring the ablation depth per laser pulse and monitoring the transition from deposited material to the substrate, LIBS (Laser-Induced Breakdown Spectroscopy) can estimate the thickness of the deposition layer [7]. However, while these measurements are precise, they are sample-based and do not allow a global in-situ evaluation of the deposition layer on the plasma-facing components in a fusion device.

☆ This article is part of a special issue entitled: 'PSI-26' published in Nuclear Materials and Energy.

* Corresponding author at: National Institute for Fusion Science, National Institutes of Natural Sciences, 322-6 Oroshi-cho, Toki, Gifu 509-5292, Japan.
*E-mail address:* motojima.gen@nifs.ac.jp (G. Motojima).

[1] See the author list in O. Grulke et al., Nuclear Fusion 64 (2024) 112002.

https://doi.org/10.1016/j.nme.2025.101934
Received 3 July 2024; Received in revised form 11 April 2025; Accepted 14 April 2025
Available online 2 May 2025

Colorimetry is less accurate than sample analysis, but can provide a global evaluation, and it is important to combine these analyses to assess the thickness of deposition layer.

The deposition layers can retain fuel particles through co-deposition. This process can impact on fuel particle control, and if the extensive distribution of deposition layers can be assessed, it would enable a better understanding of the mechanisms of layer formation and strategies to mitigate their effects. Here, each OP of W7-X is described and summarized in Table 1. More than 1000 plasma discharges were conducted in each of the three operation phases. OP1.2a was focused on testing the uncooled divertor components and verifying the general operation of the divertor system [8]. OP1.2b was aimed to improve plasma performance and explore the feasibility of long-pulse operations with uncooled divertor components [9]. OP2.1 has been marked the introduction of actively cooled divertors, enabling experiments with higher heat loads and longer plasma pulses [10]. The details of the plasma-facing components and plasma durations in W7-X are provided in [11,12]. For the wall conditioning, the details are provided in [13–16]. As for the detailed of the modules, the diagnostic used to measure the temperature and its field, the details are provided in [17–21].

Currently, in W7-X, the color analysis was conducted until the previous plasma campaign OP1.2 in which test divertor modules were installed [4]. However, since the operation campaign OP2.1, a water-cooled divertor with cryo-pumps is established, removing of the divertor tiles is no longer possible. Colorimetry can be one of the complementary measurement techniques in such cases since, with handheld device, easy in-situ measurement in the plasma-vessel is possible.

This study shows the colorimetry measurements after OP2.1 operation in W7-X. In the following section, the experimental setup is described in Section 2. In section 3, the experimental results are shown. In section 4, the considerable qualitative reasons are discussed. A summary for the colorimetry measurements after OP2.1 are drawn in section 5.

## 2. Experimental setup

This section describes a method for evaluating the thickness of deposition layers accumulated on first wall panels. The novelty of this measurement lies in the ability to assess the distribution of extensive deposition layers through reflection measurements using a portable color analyzer within a vacuum chamber. The color analyzer is equipped with an integrated LED sphere, capable of irradiating the object with a uniform standard light source. A distinctive feature of this color analyzer is its ability to measure the reflectivity of glossy metallic surfaces. For details on measurements taken with LHD, W7-X, QUEST, etc., previous papers above mentioned are referenced [2–4]. Such extensive measurement of deposition layer distribution cannot be achieved through post-mortem analysis using samples, nor fully evaluated by global particle balance analysis. Hence, this method serves as an innovative evaluation technique that bridges the two analyses. The RGB values measured by the color analyzer are explained. The reflectivity of the object is quantitatively evaluated in the wavelength regions of Red, Green, and Blue, each to a 10-bit precision (0–1023 a.u.), and the RGB values are calculated as an average of these values. The color analyzer weighs 160 g and the measurement time is 3 s, allowing for the averaging of multiple reflectivity measurements per first wall panel, thus facilitating the assessment of reflectivity. The color analyzer is lightweight, small, and user-friendly, so that it can be easily carried into the vacuum vessel opened to the atmosphere after the plasma experiment. In addition, the measurement time is only about 3 s, which makes it possible to measure many points in a short time. Furthermore, the internal memory enables continuous data storage, and the rechargeable battery eliminates the need for a continuous AC power supply. Intensity calibration is carried out by measuring a white standard paper (matt paper (no gloss) with a whiteness of 91 % or higher) before each measurement and calibrating it to the maximum value of 1023 for the R, G and B. Here, to evaluate the accuracy of the color analyzer, we conducted color calibration using about 400 color sample books (DIC Color Guide, 19th Edition, PART1, 3) whose R, G and B values were known in advance [22]. A summary of the calibration results is shown below; the R, G and B values have an offset, and their values are all similar. The R, G, and B values have similar sensitivity characteristics, with high sensitivity in large values and low sensitivity in small values. A high RGB value indicates that the image is close to white, and a low RGB value indicates that the image is close to black, i.e. the image is more sensitive when the color is white and less sensitive when the color is black. This is similar to the human eye in general, which finds it more difficult to distinguish the difference in color between black and white. From the viewpoint of the evaluation of the deposition layer, it is desirable to have sensitivity up to the region of low RGB value, and further development of the color analyzer is expected in the future. Specifications of the color analyzer are summarized in Table 2.

The process for determining the basic thickness of the deposition layers is shown in Fig. 1(a). The reflectivity of first wall panels is evaluated using the color analyzer, and the deposition layer is assessed assuming a single layer model. The model is proposed where the thickness of the deposition layer is linked to the reflection rate [1,23]. This model assumes a straightforward structure comprising three layers: the atmospheric layer, the deposition layer, and the substrate layer [4]. The reflection rate, $R_{\mathrm{ref}}$, is defined as follows.

$$\varnothing = \frac{2\pi \mathrm{N_f} d\cos\theta}{\lambda} \tag{1}$$

$$r = \frac{r_0 + r_1 \exp(i2\varnothing)}{1 + r_1 r_0 \exp(i2\varnothing)} \tag{2}$$

$$R_{\mathrm{ref}} = |r^2| \tag{3}$$

The parameters, $\varnothing$, $\lambda$, and $\theta$ represent the phase difference, the wavelength of the incident light, and the angle of incidence, respectively. In addition, $N_f$ and $d$ correspond to the refractive index and thickness of the deposition layer, while $r$ denotes the electric field ratio of the reflected light to the incident light. The Fresnel reflection coefficients at the air-deposition layer boundary and the deposition layer-substrate boundary are denoted by $r_0$ and $r_1$, respectively. This simplified model illustrates that the reflection rate depends nonlinearly on the thickness of the deposition layer. For the light's polarization, an equal ratio of S-wave to P-wave (1:1) is assumed.

The linear relationship between RGB values and reflectivity has already been confirmed by long-term irradiated sample measurements

**Table 1**
The characteristics of each OP of W7-X experiments.

| | OP1.2a | OP1.2b | OP2.1 |
|---|---|---|---|
| **Year** | **2017** | **2018** | **2022–2023** |
| **Total plasma time (s)** | **3775** | **9054** | **15,015** |
| **total energy injected (GJ)** | **0.08** | **0.2** | **1.3** |
| **Boronization** | **No** | **Yes** | **Yes** |
| **Divertor** | **Non-cooled** | **Non-cooled** | **Active-cooled** |

**Table 2**
Specifications of the color analyzer.

| Measurement | RGB (Red, Green, Blue)HSV (Hue, Saturation, Value) |
|---|---|
| Measurement window diameter | Φ8.1 mm |
| Internal diameter of integrating sphere | Φ47 mm |
| Light source | White LED |
| RGB range | 0 ~ 1023 |
| Weight | ~160 g |
| Measurement time | 3 s |
| Record | USB memory installed in analyzer |

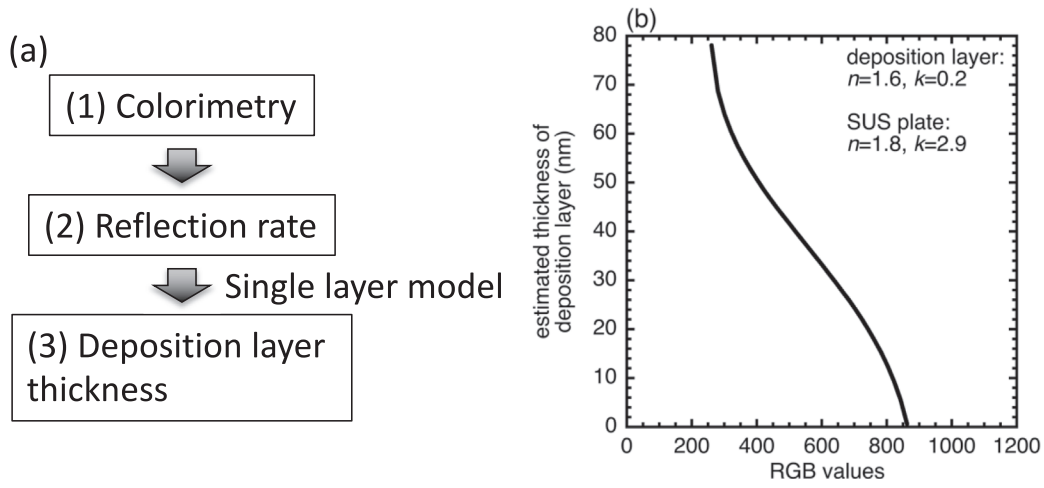


**Fig. 1.** (a) The process for evaluating the thickness of deposition layers formed on first wall panels using colorimetry. The reflection rate is assessed by colorimetry, and the deposition layers are then evaluated using a single layer model. (b) Illustrates the relationship between the estimated thickness of the deposition layers and RGB values. Here, the RGB values are the averages of the red, green, and blue values measured by colorimetry and are equivalent to the reflection rate.

in LHD [2]. The assumptions for the single layer model about the refractive index of both the stainless steel of the first wall panel substrate and the deposition layer. The values (the refractive index of the deposition layer is set to $n = 1.6$ and $k = 0.2$. For the stainless steel substrate, the refractive index is assumed to be $n = 1.8$ and $k = 2.9$) previously used for OP1.2a and OP1.2b in W7-X have been adopted for this purpose [4]. The relationship between RGB values and deposition layer thickness is shown in Fig. 1(b). The refractive index is set as carbon for the composition of the deposition layer. However, the composition of the deposition layer might be changed due to the boron coating by boronization, and the different refractive index may influence the estimation of the thickness of the deposition layer, but this is assumed to have no effect in this paper (discussed later).

Systematic measurements were conducted inside the vacuum chamber during the atmospheric opening after the completion of experiments OP1.2a and OP1.2b in W7-X. This paper presents the results of reflectivity measurements on first wall panels following the concluded OP2.1 experimental campaign. The characteristics of systematical evaluation of deposition layers thus could enhance the importance of this measurement.

## 3. Experimental results

### 3.1. Colorimetry measurements on the first wall panels for OP2.1

The CAD drawings of color pattern of the first wall panels in the recent plasma campaign OP2.1 and for the comparison in OP1.2a and OP1.2b are shown in Fig. 2. Here, abbreviation HM represents a half module. Systematic color pattern through each experimental campaign can be seen. The color is brighter in OP1.2a, compared with in OP1.2b and OP2.1. Brighter color means higher reflection rate and higher RGB values, indicating thinner deposition layer. On the other hand, darker color means lower reflection rate and lower RGB values, indicating thicker deposition layer. For generating these color patterns for an individual wall panel, an average value of the RGB measurements on that panel is considered. These color patterns show, the deposition layer of smaller thickness during OP1.2a and larger thickness during OP1.2b and OP2.1. Similar color pattern for OP2.1 and OP1.2b, indicate comparable thickness of deposition layer during these plasma campaigns.

The thickness of the deposition layer averaged over all the first wall panels estimated from colorimetry measurements after OP2.1 is shown in Fig. 3. The averaged thicknesses for OP1.2a and OP1.2b are also

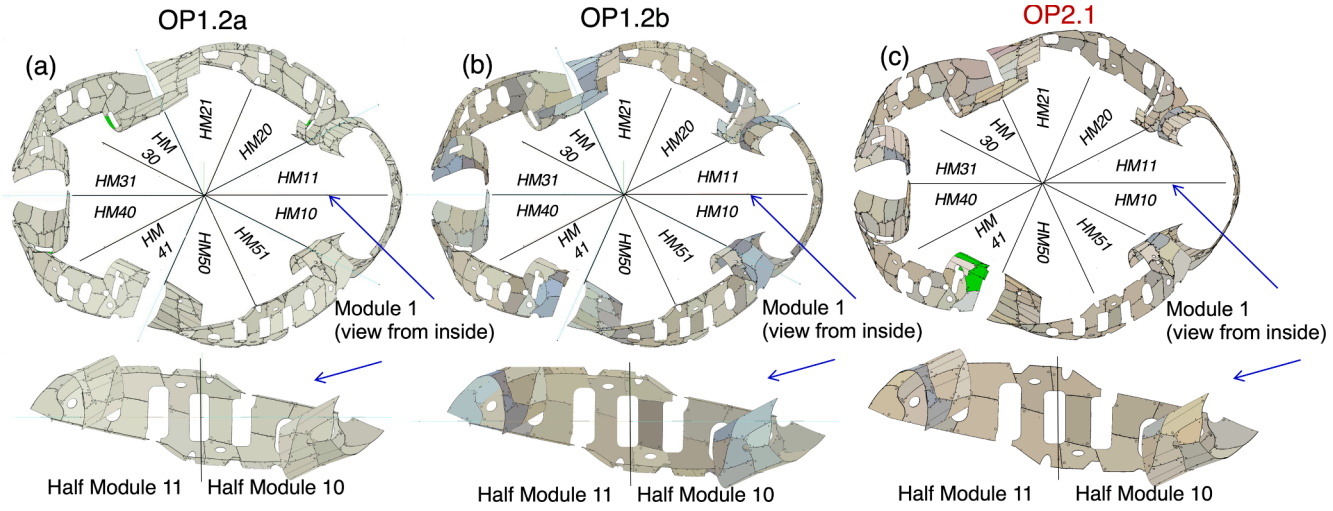


**Fig. 2.** Color patterns of first wall panels on (a) OP1.2a, (b) OP1.2b and (c) OP2.1. Systematic color pattern through each experimental campaign can be seen. The first wall panels which were not measured are shown in green color in (c). (For interpretation of the references to color in this figure legend, the reader is referred to the web version of this article.)

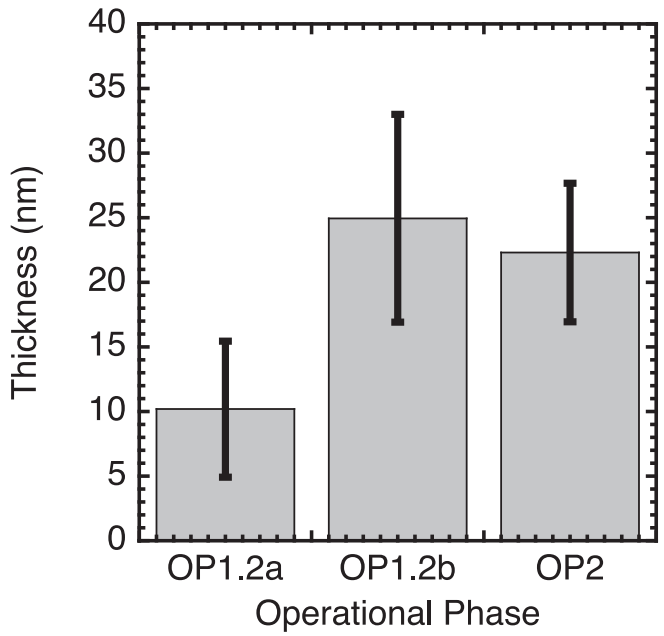


**Fig. 3.** Evaluation of the deposition layer on first wall panels through systematic reflectance measurements via colorimetry. The average thickness of the net deposition layers for operational phases OP1.2a, OP1.2b, and OP2.1 are shown. The data represent the averaged thickness of deposition layers across approximately 200 first wall panels.

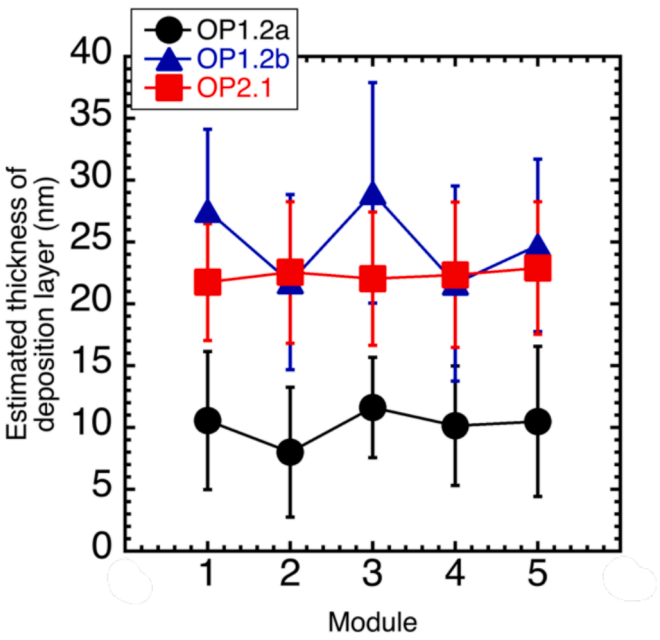


**Fig. 4.** Averaged thickness of deposition layers formed on first wall panels assessed in each module after operational phases OP1.2a, OP1.2b, and OP2.1. During OP2.1, the thickness across the modules appears uniform. In comparison to OP1.2b, there seems to be a reduction in thickness in Modules 1 and 3.

shown in the same figure. It should be noted that the thickness is an accumulation over each experimental campaign. The average estimated thickness is 10 ± 6 nm for OP1.2a and 25 ± 8 nm for OP1.2b. In OP2.1, it is estimated at 22 ± 8 nm. Thus, OP2.1 has slightly reduced thickness compared to OP1.2b. Unfortunately, in Module 4, the measurements could not be conducted on 8 panels out of 40 panels (i.e. 20 %) due to the lack of a temporary support structure to be built to access these panels. The average thickness of the deposition layer for all panels, excluding these eight panels is evaluated to be 10 ± 5 nm for OP1.2a and 25 ± 8 nm for OP1.2b, these values are comparable to the overall average values shown in Fig. 3, Therefore, it appears that the contribution of the missing 8 panels is not so significant for the average value for OP2.1.

Here, the average thickness of the deposition layer in each module is plotted in Fig. 4. In OP1.2b, the average thickness of the deposition layer is relatively thicker than the other modules, especially for Module 1 and Module 3. In OP2.1, on the other hand, the average deposition layer appears to be uniformly formed for all modules. Given that the source of carbon transported to the first wall panels is the carbon divertor, this suggests that the heat flux (or chemical sputtering) to the divertor may have been symmetrized for some reasons in OP2.1. Conversely, it is possible that in OP1.2b, the heat flux (or chemical sputtering) was asymmetric with respect to the module.

### 3.2. *Colorimetry of vertical divertor target*

The evaluation of deposition layers formed on first wall panels by colorimetry is conducted using a single layer model of the stainless steel substrate of the first wall panel and the carbon deposition layer. Evaluating these layers becomes challenging when the composition of the carbon divertor matches that of the deposition layer, making it generally difficult to assess erosion and deposition on the surface of the carbon divertor via colorimetry. Interestingly, the measurement of the reflectivity of the carbon divertor surface reveals different RGB values in each experimental phase. Systematic reflectivity measurements of vertical target of the divertors in Module 4 have been conducted during phases OP1.2a, OP1.2b, and OP2.1, as shown in Fig. 5. Although OP1.2a and OP1.2b use the same target plate made of fine grain graphite, a new water-cooled divertor made of carbon fiber-reinforced composite was installed for OP2.1. Clear patterns, which appear to complement the footprints seen in infrared camera measurements [12], are observable in OP1.2a and OP2.1. However, it is not currently conclusive whether changes in reflectivity and optical properties on the graphite divertor surface in OP1.2a are due to erosion or deposition, as these patterns disappear in OP1.2b, complicating their interpretation. A typical poloidal distribution is presented in Fig. 6, with a more pronounced peak in distribution during OP2.1. Assuming that the RGB values in OP1.2a and OP2.1 complement the divertor footprint, a comparison with LIBS results from OP1.2a suggests that high RGB value distributions may reflect the amount of erosion [7]. Given the narrower range of high RGB values in OP2.1, it may be inferred that erosion is generally less significant compared to OP1.2a. However, these interpretations are tentative and require validation against other measurements for higher possibility.

Fig. 5 shows very low RGB levels in OP1.2b on the lower and upper divertor while Fig. 3 shows higher deposition layer thickness on first wall panels in the same operating phase (with fine grain graphite components). The erosion of carbon from the divertor plates should be the source of the deposition layer. In this context, the present results may not be indicative of high RGB values indicating high erosion. For example, molybdenum polishment has resulted in improved reflectivity [24]. These examples illustrate that higher degrees of polishing lead to smoother surfaces, thereby increasing reflectivity by enhancing specular reflection and reducing diffuse scattering.

## 4. Discussions

In this section, the possible reasons are discussed for the obtained experimental results. However, it should be noted that the following discussions require further quantitative evaluations to make definitive conclusions.

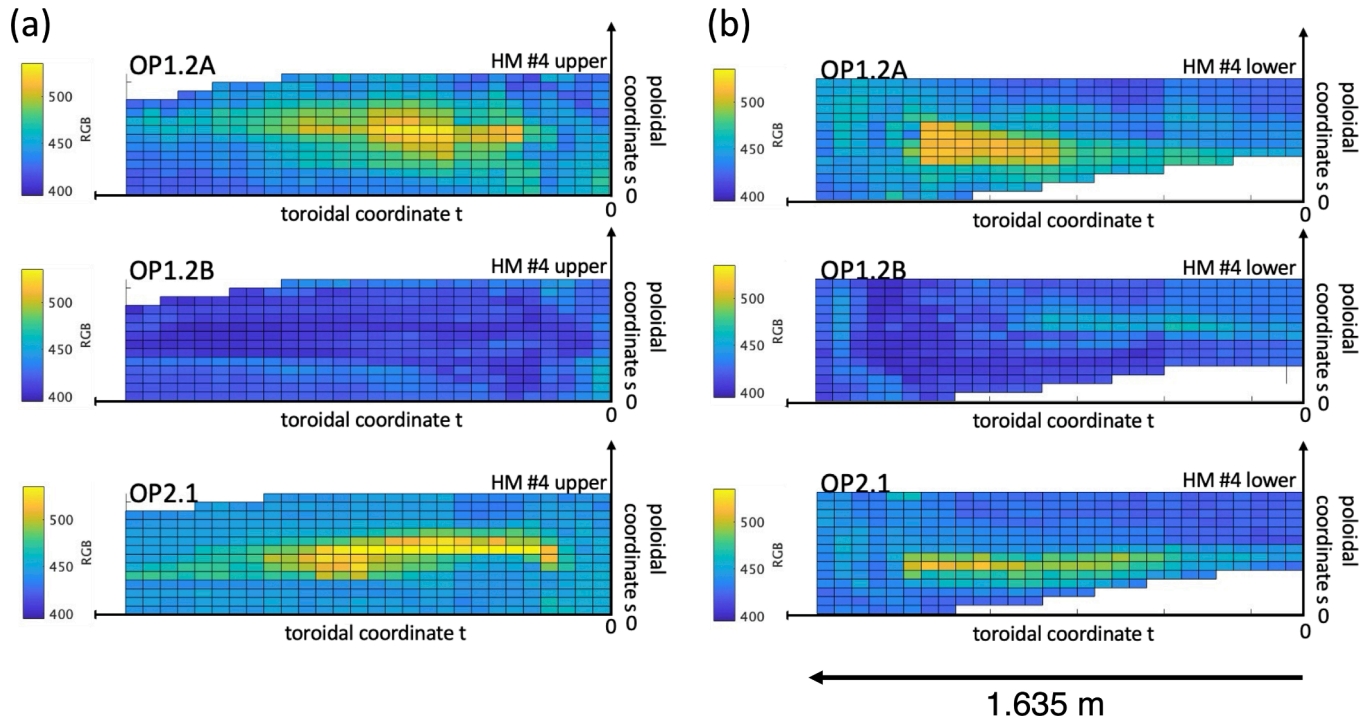


**Fig. 5.** The color patterns for (a) the upper vertical divertor and (b) the lower vertical divertor of module 4 after operational phases op1.2a, op1.2b, and op2.1. in op1.2a and op2.1, structures showing distinct footprints are visible.

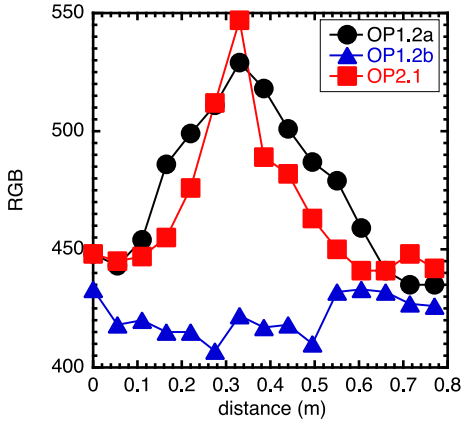


**Fig. 6.** The poloidal distribution of typical RGB values during operational phases OP1.2a, OP1.2b, and OP2.1. In OP2.1, the width of the distribution appears more peaked compared to OP1.2a.

### *4.1. Lower surface temperature of the divertor target elements in OP2.1*

In the recent publication by Naujoks et al [ref. 25], Fig. 7 is referenced to compare the surface temperature and heat load near the divertor target for operation phases OP1.2b and OP2.1, both at the same heating power (ECH ~ 5 MW). The study highlights that the heat flux and heat load are significantly reduced—by 2 to 3 times—in OP2.1 compared to OP1.2b, at the baffle module BM1v (as shown in dotted line in Fig. 7(c) and (d)) due to the new geometric design of the tiles using tungsten. This reduction is also evident in the water cooled Carbon Fiber-reinforced Composite (CFC) divertor target elements during OP2.1, during OP1.2b these were enertially cooled fine grain graphite target elements. The data suggests that lower temperatures may result in decreased sputtering to the divertor plate during OP2.1, potentially leading to suppressed formation of the deposition layer on the first wall panels. On the other hand, a total discharge lengths are about 15,015 s in OP2.1, 9,054 s in OP1.2b and 3,775 s in OP1.2a as shown in Table 1. This means that despite the increase in accumulative discharge time, OP2.1 seems not to be seen the formation of a deposition layer. This effect likely contributes to a deposition layer distribution in OP2.1, similar to that observed in OP1.2b, possibly due to the incorporation of a water-cooled divertor system. This change in design could enhance the stability and efficiency of operations by reducing the thermal stress on the divertor components. Also, it might be possible to consider that the erosion of charge exchange neutrals at the wall panels is more dominant in OP2.1 than the deposition of impurities such as carbon, resulting in less (net) deposition on the panels and even in net erosion of the 'old' OP1.2 layers. Thus, the investigation of the balance between deposition and erosion by colorimetry might contribute to the understanding of the balance between the soure term and charge neutlals, which is important for the modeling. However, unfortunately in W7-X there are neither any measurements of charge exchange neutral flux of fuel species nor the simulations available.

The chemical erosion of amorphous hydrogenated carbon films by thermal hydrogen neutral increases strongly with increasing temperature, goes through a maximum and rolled over around 650–700 K [26]. Also, it is reported that the chemical sputtering of graphite due to bombardment with hydrogen ions increases with increasing target temperature, reaches a maximum in the range of about 900 K, and decreases for further increasing temperature [27]. However, because the chemical sputtering is coupled strongly with the other forms of sputtering, therefore, for correlating the chemical sputtering alone with the net erosion on the wall panels interpreted by the colorimetry measurements might be difficult. Fig. 7 shows the higher divertor temperatures observed in OP1.2b, in contrast to the lower temperatures observed in OP2.1. A more detailed view is drawn in Fig. 8, which shows the time evolution of the divertor temperature measured by Infrared camera (IR) thermography [28,29] for OP1.2a, OP1.2b, and OP2.1. A representative day with the standard magnetic configuration has been selected for these plots. The temperature values correspond to the divertor target modules (TM2h + TM3h) and represent the average across these modules, where the main strike line is located. It is seen that for OP1.2a and

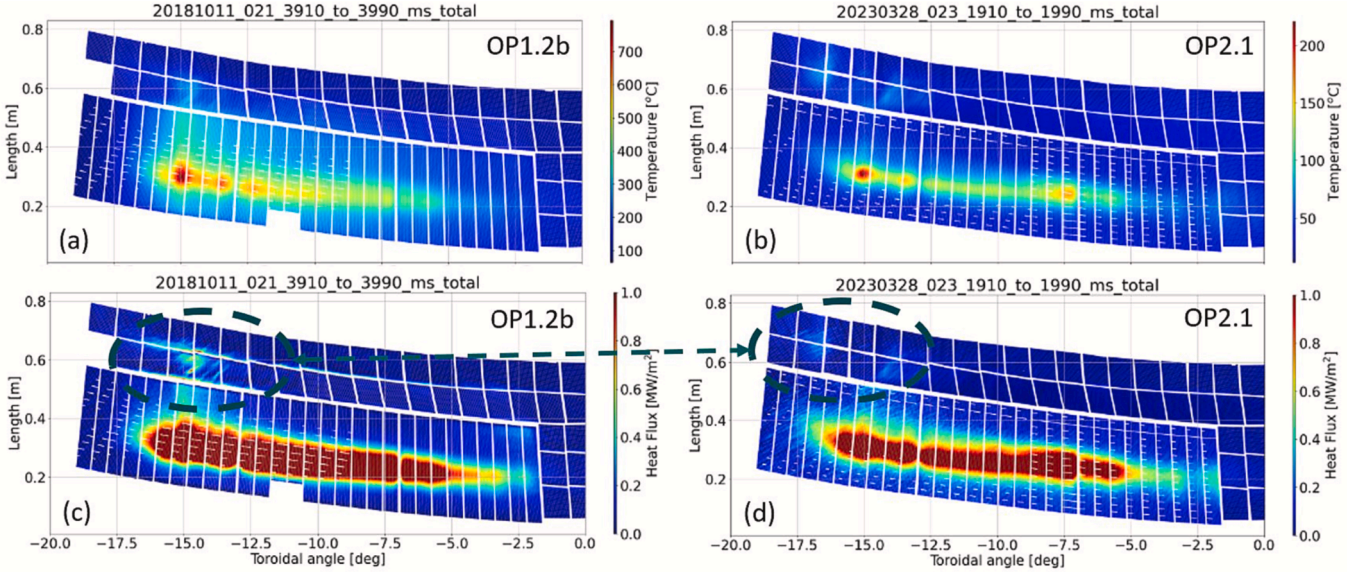


**Fig. 7.** Comparison of surface temperature and heat load pattern for the vertical divertor target in OP1.2b and OP2.1. This figure is reproduced from the reference paper [25]. Here the difference in surface temperatures in OP1.2b and OP2.1, or the width of heat load pattern is discussed. The discharge number together with the time duration for the shown measurement is given above each figure. BM1v is shown in dotted line in Fig. 7(c) and (d).

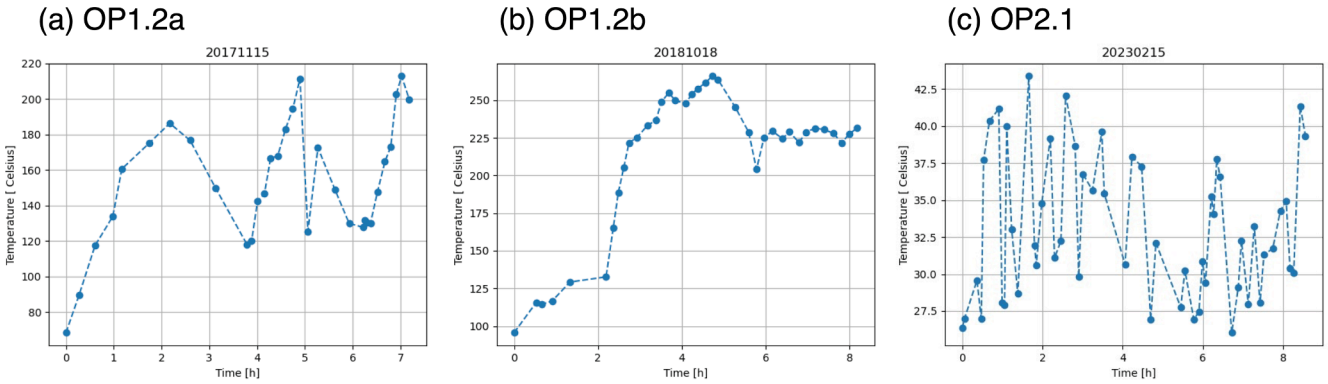


**Fig. 8.** Time evolution of the divertor temperature measured by IR thermography for (a) OP1.2a, (b) OP1.2b, and (c) OP2.1. The X-axis represents the time (in hours) over a day, while the Y-axis shows the average temperature of the divertor target modules (TM2h + TM3h), averaged over these modules. These are the average temperature values for the nine divertor modules, one is missing due to unavailability of IR camera measurements. This averaging takes into account the asymmetry of the heat loads on the upper and lower divertors. Each data point represents a discharge, with the surface temperature taken at the moment when the heating power is turning off.

OP1.2b with uncooled divertor the heat is accumulated over the day and the temperatures increases above 200 °C, however, for OP2.1 with water cooling, the temperature drops after each discharge and remains below 43 °C even during the discharge with the surface temperature balanced by the water cooling. Consequently, chemical erosion is expected to be more significant in OP1.2a and OP1.2b, where the divertor targets are considerably hotter, compared to OP2.1 under similar heat load conditions. Radiation Enhanced Sublimation (RES) might be also one of the contributing factor [30]. However, the RES often occurs over 2200 K, therefore the contribution might not be dominant in the actual divertor temperature.

### 4.2. Lower impurity level

It has been confirmed that the concentration of oxygen and carbon in the plasma was dramatically reduced after three boronizations in OP1.2b. In OP2.1, five boronizations were performed [14], and it is possible that the impurity level is further reduced in OP2.1 and that the carbon sputtering of the divertor plates due to impurity might be suppressed. Carbon line radiation was decreased by several factors by boronization which getters oxygen on the plasma facing walls, while boron line radiation was increased. Due to decreased impurity radiation at the edge, density limit is increased, operation above $10^{20}$ $m^{-2}$ is enabled. Higher line integrated density was achieved with same ECH power.

Alternatively, if the water-cooled divertor newly installed in OP2.1 originally contained fewer impurities such as $H_2O$, this may have affected the suppression of carbon deposition layer formation.

The refractive index of a boron film is $n = 3.1$, $k = 0.2$ (at 0.6 μm) [31]. Amorphous boron exhibits relatively inhomogeneous electronic structure and optical properties, leading to variations in its bandgap and refractive index. In this study, we refer to the optical properties of $\beta$-rhombohedral boron. Assuming a deposition layer with this refractive index and applying the single-layer model, the thickness of the deposition layer is expected to decrease. Although not all deposition layers are necessarily composed entirely of boron, assuming full boron composition, the layer thickness is estimated to decrease by approximately 0.1–0.3 times. While the refractive index of the deposition layer for OP1.2a has been evaluated, it is necessary to assess and discuss the actual composition of the deposition layer in OP2.1.

### 4.3. Location of sputtered carbon source

The transport of carbon may be affected by the magnetic field configurations in the experiment. In OP2.1, experiments were conducted with various magnetic field configurations. Detailed analysis is required to determine the proportion of standard configurations and different configurations, and how much the proportion differs compared to OP1.2b. However, if carbon transport is different in OP2.1, it is quite possible that it affects the formation of the first wall deposition layer.

## 5. Conclusion

Using colorimetry, it was determined that the average thickness of deposition layers formed on the systematic first wall panels during operational phases OP1.2b and OP2.1 showed no significant difference. The average estimated thickness is $10 \pm 6$ nm for OP1.2a and $25 \pm 8$ nm for OP1.2b. In OP2, it is estimated at $22 \pm 8$ nm. This suggests that the net formation of deposition layers on first wall panels during OP2.1 was reduced. The balance of deposition and erosion of deposition layer on the first wall panels is presumably changed in OP2.1. The reduction in sputtering from the carbon divertor, which is the primary source of the deposition layers, could be considered for OP2.1. This phase featured a water-cooled divertor, which likely influenced these results. Moreover, the clear pattern of the colorimetry on the divertor target elements is seen in OP1.2a and OP2.1 not in OP1.2b. However, it is not currently conclusive whether changes in reflectivity and optical properties on the graphite divertor surface are due to erosion or deposition.

This outcome could positively impact particle control in the long-duration discharges planned for future W7-X experiments. In comparison, in LHD's long-duration discharges, co-deposition of fuel particles during layer formation has been observed, with fuel particles being retained by the plasma-facing walls and dynamic particle retention characteristics seen with changes in divertor plate temperatures, highlighting difficulties in particle control [32]. Therefore, the results indicating suppressed layer formation in OP2.1 could facilitate particle control. Moreover, enhanced utilization of divertor pumping could further improve particle control capabilities. In future, post-mortem analysis on sample on the first wall to identify the composition of the layer (B or C, or B, C mixture) is important to make the evaluation of deposition layer from colorimetry improved.

## CRediT authorship contribution statement

**G. Motojima:** Writing – original draft, Visualization, Project administration, Methodology, Investigation, Funding acquisition, Data curation, Conceptualization. **S. Masuzaki:** Writing – review & editing, Methodology, Investigation, Data curation, Conceptualization. **C.P. Dhard:** Writing – review & editing, Project administration, Investigation. **D. Naujoks:** Writing – review & editing, Project administration, Investigation, Conceptualization. **Mattis Hänel:** Visualization. **Yu Gao:** Investigation.

## Declaration of competing interest

The authors declare that they have no known competing financial interests or personal relationships that could have appeared to influence the work reported in this paper.

## Acknowledgements

This research was supported by the International Research Exchange Support Program of the National Institutes of Natural Sciences. This work has been also carried out within the framework of the EUROfusion Consortium, funded by the European Union via the Euratom Research and Training Programme (Grant Agreement No 101052200 — EUROfusion). Views and opinions expressed are however those of the author(s) only and do not necessarily reflect those of the European Union or the European Commission. Neither the European Union nor the European Commission can be held responsible for them.

## Data availability

Data will be made available on request.

## References

[1] G. Motojima, et al., Colorimetry in nuclear fusion research, IntechOpen (2022), https://doi.org/10.5772/intechopen.101634.
[2] G. Motojima, et al., Wide-range evaluation of the deposition layer thickness distribution on the first wall by reflection coefficient measurements, Nucl. Mater. Energy 12 (2017) 1219–1223.
[3] Z. Wang, et al., Measurement of thickness of film deposited on the plasma-facing wall in the QUEST tokamak by colorimetry, Rev. Sci. Instrum. 88 (2017) 093502.
[4] G. Motojima, et al., In-vessel colorimetry of Wendelstein 7-X first wall components: variation of layer deposition distribution in OP1.2a and OP1.2b, Phys. Scr. T 171 (2020) 014054, https://doi.org/10.1088/1402-4896/ab5618.
[5] M. Rubel, et al., Overview of wall probes for erosion and deposition studies in the TEXTOR tokamak, Matter Radiat. Extremes 2 (2017) 87–104.
[6] M. Mayer, et al., Carbon erosion/deposition on the divertor of W7-X during the operational period OP 1.2b, Nucl. Fusion 62 (2022) 126049, https://doi.org/10.1088/1741-4326/ac94e2.
[7] D. Zhao, et al., Investigation of boron distribution and material migration on the W7-X divertor by picosecond LIBS, Phys. Scr. 97 (2022) 024005.
[8] T.S. Pedersen, et al., First divertor physics studies in Wendelstein 7-X, Nucl. Fusion 59 (2019) 096014.
[9] T.S. Pedersen, et al., Experimental confirmation of efficient island divertor operation and successful neoclassical transport optimization in Wendelstein 7-X, Nucl. Fusion 62 (2022) 042022.
[10] C. P. Dhard, et al, "Plasma-wall interaction, exhaust and wall conditioning studies in the stellarator Wendelstein 7-X with actively cooled high heat flux divertor and experiments with tungsten PFCs", Presented in 8th Asia-Pacific Conference on Plasma Physics, 2024. https://www.aappsdpp.org/DPP2024/html/3contents/pdf/5559.pdf.
[11] C.P. Dhard, et al., Plasma-wall interaction studies in W7-X: main results from the recent divertor operations, Phys. Scr. 96 (2021) 124059.
[12] S. Brezinsek, et al., Plasma–surface interaction in the stellarator W7-X: conclusions drawn from operation with graphite plasma-facing components, Nucl. Fusion 62 (2022) 016006.
[13] R. Brakel, et al., Strategy and optimisation of wall conditioning at the Wendelstein 7-X stellarator, in IAEA Fusion Energy Conference Gandhinagar, India, IAEA, 22–27 October (2018). Paper No. IAEA-CN-258/EX/P8-17.
[14] L. Vano, et al., Wall conditioning in preparation for long pulse operation at the Wendelstein 7-X stellarator, 49th European Conference on Plasma Physics, Poster No. 1094 (2023).
[15] T. Wauters, et al., Wall conditioning by ECRH discharges and He-GDC in the limiter phase of Wendelstein 7-X, Nucl. Fusion 58 (2018) 066013.
[16] A. Goriaev, et al., Wall conditioning at the Wendelstein 7-X stellarator operating with a graphite divertor, Phys. Scr. T171 (2020) 014063.
[17] R. König, et al., Diagnostic design for steady state operation of the W7-X, Rev. Sci. Instrum. 81 (2010) 10E133.
[18] H.-S. Bosch, et al., Technical challenges in the construction of the steady state stellarator W7-X, Nucl. Fusion 53 (2013) 126001.
[19] T. Sunn Pedersen, et al., Confirmation of the topology of the Wendelstein 7-X magnetic field to better than 1:100 000, Nat Commun 7 (2016) 13493.
[20] O. Grulke, et al., Overview of the first W7-X long pulse campaign with fully water-cooled plasma-facing components, Nucl. Fusion 64 (2024) 112002.
[21] T. Klinger, et al., Overview of first W7-X high performance operation, Nucl. Fusion 59 (2019) 112004.
[22] G. Motojima, et al., Preliminary examination of reflection coefficient measurement of RGB lights on the first wall in LHD, Plasma Fusion Res. 10 (2015) 1202074.
[23] O.S. Heavens, Optical properties of thin films, Rep. Prog. Phys. 23 (1960) 1.
[24] A.E. Gorodetsky, et al., Effect of techniques for polishing molybdenum mirrors on their optical stability under cleaning D2–N2 plasma, J. Surf. Investig. 14 (2020) 1003–1015.
[25] D. Naujoks, et al., Performance of tungsten plasma facing components in the stellarator experiment W7-X: Recent results from the first OP2 campaign, Nucl. Mat. Ene. 37 (2023) 101514.
[26] M. Schluter, et al., Temperature dependence of the chemical sputtering of amorphous hydrogenated carbon films by hydrogen, J. Nucl. Mater. 376 (2008) 33–37.
[27] W. Jacob, J. Roth, Chemical Sputtering, in: Sputtering by Particle Bombardment, Topics in Applied Physics, vol. 110, Springer, Berlin, Heidelberg, 2007, https://doi.org/10.1007/978-3-540-44502-9_6.
[28] M. Jakubowski, et al., Infrared imaging systems for wall protection in the W7-X stellarator (invited), Rev. Sci. Instrum. 89 (2018) 10E116.
[29] Y. Gao, et al., Methods for quantitative study of divertor heat loads on W7-X, Nucl. Fusion 59 (2019) 066007.

[30] J. Roth, D. Garcia-Rosales, Analytical description of the chemical erosion of graphite by hydrogen ions, Corrigendum, Nucl. Fusion 37 (1997) 897.
[31] Nobuyoshi Morita, Akira Yamamoto, Optical and Electrical Properties of Boron, Jpn. J. Appl. Phys. 14 (1975) 825.
[32] G. Motojima, et al., Global helium particle balance in LHD, J. Nucl. Mater. 463 (2015) 1080.